

Article

Implementation of Fluidized Bed Concept to Improve Heat Transfer in Ecological Adsorption Cooling and Desalination Systems

Karolina Grabowska ^{1,*}, Jaroslaw Krzywanski ¹, Anna Zylka ¹, Anna Kulakowska ¹, Dorian Skrobek ¹, Marcin Sosnowski ¹, Radomir Ščurek ², Wojciech Nowak ³ and Tomasz Czakiert ⁴

¹ Faculty of Science and Technology, Jan Dlugosz University in Czestochowa, Armii Krajowej 13/15, 42-200 Czestochowa, Poland; j.krzywanski@ujd.edu.pl (J.K.); a.zylka@ujd.edu.pl (A.Z.); a.kulakowska@ujd.edu.pl (A.K.); d.skrobek@ujd.edu.pl (D.S.); m.sosnowski@ujd.edu.pl (M.S.)

² Institute of Intelligence Studies, University of Defence, Kounicova 65, 662 10 Brno, Czech Republic; radomir.scurek@unob.cz

³ Faculty of Energy and Fuels, AGH University of Science and Technology, A. Mickiewicza 30, 30-059 Cracow, Poland; wnowak@agh.edu.pl

⁴ Department of Advanced Energy Technologies, Czestochowa University of Technology, Dabrowskiego 73, 42-201 Czestochowa, Poland; tomasz.czakiert@pcz.pl

* Correspondence: k.grabowska@ujd.edu.pl

Abstract: Sustainable development policy focuses on reducing the carbon footprint generated by the global industry and energy sector. Replacing conventional energy sources with environmentally friendly ones requires advanced research to increase energy efficiency and reduce the instability and intermittence of renewable sources. Moreover, adsorption chillers are an opportunity to introduce net-zero emission technologies to the refrigeration, air-conditioning, and desalination industries. Adsorption devices could be popularized if a method of effective heat transfer in the volume of the adsorption bed is developed. The innovative concept of introducing fluidized beds into the adsorption system can achieve the most promising results in improving energy efficiency. To confirm the adopted assumption, heat transfer coefficient calculations for the packed and fluidized bed were carried out in this paper based on experimental tests and literature data. The empirical research aims to extend the fundamental knowledge in the implementation of fluidization under low-pressure conditions, characteristic of the adsorption systems' working cycle. Experiments were conducted on a unique test stand equipped with the Intensified Heat Transfer Adsorption Bed (IHTAB) reactor prototype. Five adsorption bed samples were analyzed. The reference sample consisted only of silica gel, and the subsequent ones contained aluminum or carbon nanotubes with 5 and 10% additions. In the case of samples with admixtures, the fluidized state increased the heat transfer coefficient on average from approx. 36.9 W/m² K to approx. 245.4 W/m² K.

Keywords: net-zero emission; heat transfer coefficient; fluidized bed; energy efficiency; adsorption cooling and desalination systems; adsorption bed



Citation: Grabowska, K.; Krzywanski, J.; Zylka, A.; Kulakowska, A.; Skrobek, D.; Sosnowski, M.; Ščurek, R.; Nowak, W.; Czakiert, T. Implementation of Fluidized Bed Concept to Improve Heat Transfer in Ecological Adsorption Cooling and Desalination Systems. *Energies* **2024**, *17*, 379. <https://doi.org/10.3390/en17020379>

Academic Editor: Annunziata D'Orazio

Received: 6 December 2023

Revised: 29 December 2023

Accepted: 9 January 2024

Published: 12 January 2024



Copyright: © 2024 by the authors. Licensee MDPI, Basel, Switzerland. This article is an open access article distributed under the terms and conditions of the Creative Commons Attribution (CC BY) license (<https://creativecommons.org/licenses/by/4.0/>).

1. Introduction

The global sustainable development policy towards a zero-carbon economy demands changes in all industry sectors [1]. Implementing ecological technologies in the energy sector will be a crucial challenge in the coming years to achieve a net-zero emission economy. Moreover, worldwide sustainable development policy requires a radical and immediate reduction in fossil fuel exploitation by renewable energy sources in various areas of societies' operation [2,3]. Significant attention is being paid to reducing the carbon footprint generated in the production process, transportation, or service sectors [4,5]. First, the high carbon footprint characterizes energy-consuming technologies, such as

conventional refrigeration technology, which is becoming more common due to the global warming effect [6,7].

Adsorption chillers provide an opportunity to introduce ecological solutions in the refrigeration, air-conditioning, and desalination industries [8,9]. The growing interest in adsorption desalination technology results from disturbing forecasts of increasing freshwater deficits in various parts of the Earth. According to the UN, by 2030, $\frac{1}{4}$ of the world's population will be affected by water scarcity due to permanent or temporary droughts, and around 50 million people will have to emigrate due to freshwater deficits [10,11]. These disturbing data influence the need to develop sustainable desalination methods, which include adsorption technology. However, there are still few literature reports related to research on improving the efficiency of adsorption desalination systems [12,13]. The potential of solar water desalination systems consisting of a simple design and plentiful rectangular troughs in desalination under vacuum conditions has been explored in [14,15] due to the high solar intensities and long sunshine duration in Saudi Arabia. The net-zero emission potential of adsorption refrigeration and desalination is related to the possibility of using low-grade thermal sources for power, such as industrial waste heat, solar and wind energy, heat produced in cogeneration, and geothermal heat [16–18].

The adsorption device consists of three main parts: an evaporator, an adsorption bed, and a condenser. The number of individual components can be increased to compose the multi-bed systems of multi-stage operating cycles [19,20]. The working cycle of an adsorption refrigerator begins with the process of refrigerant evaporation. Then, the evaporator is connected to the adsorption bed, where the produced water vapor is adsorbed on the porous medium surface. An exothermic adsorption requires constant heat removal to maintain the process dynamics. Therefore, cooling water flows through the heat exchanger system built into the bed volume while adsorption is carried out. At this stage, the bed chamber has no connection with the condenser. When the sorbent bed is saturated, the valve connecting the evaporator with the bed is closed, and the preheating process begins, leading to the desorption of the water vapor. The hot water is supplied to the exchanger built into the bed due to the endothermic character of desorption, and the bed chamber remains disconnected from both the evaporator and the condenser. After that, the desorbed refrigerant is directed to the condenser, where, after condensation, it goes back to the evaporator, and the adsorption bed is pre-cooled to prepare the adsorbent for the next adsorption cycle [21].

This technology could be popularized if a method of effective heat transfer in the volume of the adsorption bed is developed, allowing for reductions in the production and deployment costs of a highly energy-efficient adsorption cooling system [22,23].

The analyzed methods of improving thermal conditions in the adsorption bed include coated and polydisperse structures of fixed beds (packed beds). A coated sorbent layer could be implemented to reduce the thermal resistance at the boundary of sorbent grains and the heat exchanger surface. The effect of using coated beds and packed beds on adsorption system performance was discussed in [24,25]. It was investigated that the coated bed thermal parameters can be improved with the optimal selection of the coating thickness, grain size, and highly conductive binder used. Moreover, the experimental research cycles conducted in [26,27] allowed for selecting optimal adhesive materials and then for experimental confirmation of their thermal properties in coated adsorption bed constructions. The silica gel and sodium polyacrylate desiccants were coated onto a finned tube heat exchanger in the adsorption dehumidification system. The adsorbent was coated on the fins, allowing the fixed fin area to be coated with greater amounts of desiccants for better dehumidification performance [28,29].

Various configurations of heat exchangers with an expanded heat exchange surface were examined in [30,31]. The different fin constructions and geometries, the heat exchanger materials, and the ratio of the metal mass to the overall sorbent mass are analyzed in the literature because the high metal content causes a decrease in the sorption capacity of the bed [32,33]. Experimental research in the field of materials engineering is also ongoing

regarding the possibility of utilizing novel sorbents with precisely designed thermal and sorption properties [34–36].

The doping of adsorption beds with materials of higher thermal conductivity [32,37] and the construction of polydisperse beds with reduced porosity are also discussed in the literature. The influence of the spatial porosity distribution in the z direction was described in [38]. Provided the bed porosity increased from the cooling side to the steam side, the overall heat transfer performance was improved, reducing the adsorption temperature that contributes to the adsorption uptake and the Specific Cooling Power (SCP).

Moreover, the most popular investigated methods constitute implementing multi-bed devices and multi-stage sorption cycles and employing a re-heating scheme [39,40]. The implementation of heat and mass recovery schemes yields higher performance. In the three-bed mass recovery chiller, the first two beds are in the mass recovery process isolated from both the evaporator and condenser. At the same time, a third bed is connected with the evaporator to enhance cooling capacity. There are also scientific reports of integrating adsorption devices with absorption systems (AD-AB systems) to achieve greater efficiency [41,42]. However, these and other innovations in sorption technologies still require numerous experimental and numerical verifications using advanced computational methods, enabling the initial verification of the possibility of implementing innovative solutions and evaluating their effectiveness [33,43]. The prediction of the thermal conductivity of nanofluids has been successfully carried out in [44] using experimental correlation and artificial neural networks. A numerical comparison of heat transfer conditions in coated and fixed (packed) beds was carried out in [45].

One of the latest methods investigated to improve heat transfer in adsorption chillers is the implementation of fluidized beds [46]. Fluidization allows for a significant increase in the heat transfer coefficient, which is confirmed by the vast industrial application of this technology [47,48]. In [49], the coal and syngas combustion method in a circulating fluidized bed (CFB) was presented. Adsorption processes in fluidized bed columns were analyzed in [50]. A fluidized bed dryer was examined in [51,52] to explore the efficient drying of biomass.

Only a few experimental reports are currently available in the literature on improving the energy efficiency of adsorption chillers using fluidized bed technology [53]. The influence of fluidizing gas velocities and adsorbent particle diameters was discussed in [54]. The calculations indicate that the bed-to-wall heat transfer coefficient in the adsorbent fluidized bed is much higher than in a conventional bed. For silica gels with a diameter of 150 μm , heat transfer coefficients increased from 7.87 $\text{W}/\text{m}^2 \text{K}$ in the fixed state to 103.99 $\text{W}/\text{m}^2 \text{K}$ in the fluidized state. The sorbent layer is brought into a fluidized state by a fluidizing medium: water vapor enters the bed from the evaporator due to the pressure difference that occurs during the adsorption cycle. It intensifies mixing processes in fluidized conditions, which can be observed as a significant improvement in the heat and mass transfer within the adsorption bed.

The new and unconventional experimental verification of fluidized beds introduced in this paper assesses the possibility of extending the implementation areas of this technology. It extends fundamental scientific knowledge concerning fluidization under low-pressure conditions, characteristic of the adsorption systems' working cycle, since the proposed experimental concept of implementing fluidization significantly reduces the adsorption refrigeration system dimensions. Moreover, the average values of the convective heat transfer coefficient for packed and fluidized bed samples discussed in this paper are very valuable for the rapid development of refrigeration and adsorption desalination methods, particularly given ongoing climate changes, the worldwide scarcity of freshwater, and the necessity of developing novel and sustainable technologies.

The experimental tests and calculations presented in this paper were carried out to solve the following research problems:

- Is it possible to effectively implement fluidized bed technology in the operating conditions of an adsorption cooling and desalination system?

- Does fluidized bed technology improve heat transfer conditions in adsorption beds?
- How does the composition of the adsorption bed sample in fluidized conditions affect the heat transfer parameters?

It is also worth mentioning that the calculations presented in this paper are based on experiments using an innovative prototype test stand, one of the few apparatuses in the world that allows visual observation of the fluidized state in the low-pressure regime.

2. Materials and Methods

2.1. Prototype Test Stand: Intensified Heat Transfer Adsorption Bed (IHTAB) Reactor

A unique test stand designed to develop optimal fluidization conditions for sorption materials under a low-pressure regime was used to conduct the experimental studies. The first authors' experience with the experimental tests of fluidized beds dedicated to adsorption chillers on the introduced stand was presented in [55]. The authors succeeded in the empirical analysis of the possibility of implementing the fluidization process in adsorption chillers. The utilized Intensified Heat Transfer Adsorption Bed (IHTAB) Reactor Prototype constitutes the adsorption chiller's lab-scale model and is presented in Figure 1.



Figure 1. The scheme of the experimental test stand marked with the most essential elements: 1—reaction chamber; 2—aluminum frame; 3—evaporator chamber; 4—laboratory vacuum system; 5—data acquisition and control system; 6—PC.

The IHTAB test stand consists of an adsorption chamber (1), aluminum frame (2), evaporator (3), laboratory vacuum system (4), data acquisition and control system (5), and PC (6). The chambers are made of stainless steel. The evaporator chamber is located on the lower part of the test unit, where a Welch LVS vacuum pump is also installed, to which both chambers are connected. The pump is responsible for maintaining conditions consistent with the working cycle of an adsorption chiller based on the water–silica gel system. This unique lab apparatus simulates the operation of an existing adsorption chiller by running continuous,

successive cycles of adsorption and desorption, which are the essential stages in the working cycle of commercial adsorption systems for cooling and desalination. Furthermore, the test stand allows the analysis of different adsorption systems, including those with packed beds, fluidized beds, and different heat exchanger designs.

The working cycle of the unique experimental apparatus is as follows. In the evaporator, the pressure is reduced to approximately 2500 Pa, which allows for evaporating water at a temperature of approximately 21 °C. After opening a valve between the evaporator and the adsorption chamber due to the pressure difference, the water vapor flows into the adsorption chamber, where it is adsorbed on the porous medium surface. Due to the exothermic adsorption process, an increase in the temperature of the adsorbent bed is recorded using thermocouples placed in the bed. Once pressure equilibrium is reached, the valve between the evaporator and the adsorption chamber is closed. Then, the saturated bed is desorbed to prepare it for the next adsorption cycle. The heat Q required for the endothermic desorption process is supplied using a cartridge heater. The desorbed water vapor is discharged from the adsorption chamber through a channel connecting it to the vacuum pump. Once the desorption process is complete, the next adsorption cycle of the bed begins.

The unique test stand Intensified Heat Transfer Adsorption Bed (IHTAB) Reactor constitutes a laboratory-scale model of the main working elements of an adsorption chiller, adapted to the analysis and optimization of various parameters of real adsorption systems, e.g., constructions and compositions of adsorption beds, and various operating parameters of adsorption cycles. Moreover, the chambers of the test stand were equipped with certified measuring instruments with defined measurement accuracy.

The technical parameters of the experimental test stand are shown in Table 1.

Table 1. Technical characteristics of the device [56].

Parameter	Unit	Value
Name of equipment	-	Intensified Heat Transfer Adsorption Bed (IHTAB) Reactor
Serial number	-	240/2019
Validation year	-	2019
electrical supply	(VAC)	Single-phase TN S 230 V AC network
Dimensions (width/length/height)	(mm)	1280/700/1550
Total mass	(kg)	~160
Adsorption chamber dimensions (height/diameter)	mm	520/404
Desorption chamber dimensions (height/diameter)	mm	418/404

The equipment with the parameters defined in Table 1 was designed to provide a precise laboratory test stand enabling simulation of the adsorption cooling and desalination system operation. The volume of the adsorption and evaporator chambers was 0.067 m³ and 0.054 m³, respectively. An apparatus of these dimensions enables precise laboratory-scale tests to be performed.

The equipment of the adsorption chamber is shown in Figure 2 with the cross-section.

According to Figure 2, the adsorption bed of porous media was placed inside the sorption column (3), which was located on the scale. It enabled measurement of the mass of the adsorbed water vapor. In the analyzed studies, the sorption column, with dimensions of 0.17 m in height and 0.03 m in outside diameter, was made of PLEXY PMA material with a wall thickness of 0.002 m. The dimensions and modular equipment of the adsorption chamber allowed for the examination of sorbent beds and heat exchangers of different sizes and construction. In the studied case, it was crucial to precisely verify heat transfer in fluidized and packed beds of different compositions, so a small sample size was chosen. The sorption column was limited by a grid (2) with a diameter below 50 µm to prevent

sorbent sprinkling during analysis in the fluidized condition. The grid resolution should be smaller than the diameter of the sorbent particles and the additives used to protect against undesirable loss of sample weight during experiments. Changes in the sorbent bed temperature caused by the adsorption phenomena were recorded using thermocouples placed at equal distances from the column axis (manufactured by Czaki Thermo-Product Company, Rybie, Poland, TP-203 K-1a model, accuracy $\pm 1.5\text{ }^{\circ}\text{C}$) (1). In the column axis, a heat transfer probe (manufactured by Sinkoplex Company, Ostrów Wielkopolski, Poland, type A WS) (4) was set to analyze the heat transfer conditions in the adsorption bed related to the diagnosed type of bed structure. The heat transfer probe is presented in detail in Figure 3.

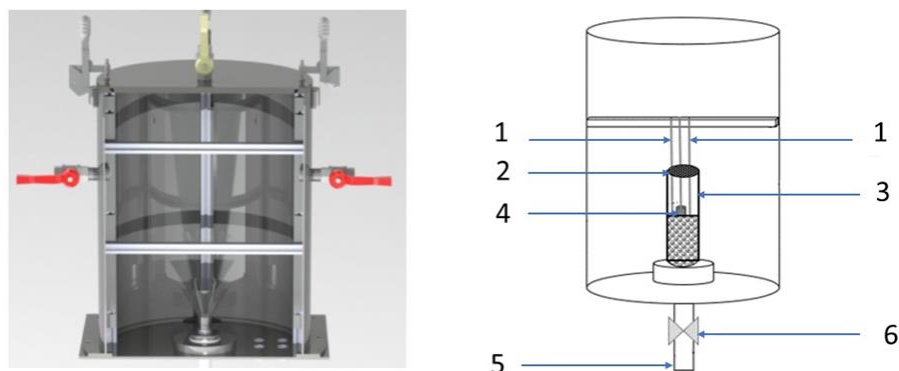


Figure 2. The cross-section of the reaction chamber with the scheme of adsorption bed equipment [56]: 1—thermo-couples; 2—grid; 3—sorption column; 4—heat transfer probe; 5—water vapor channel; 6—the valve between reaction and evaporator chamber.

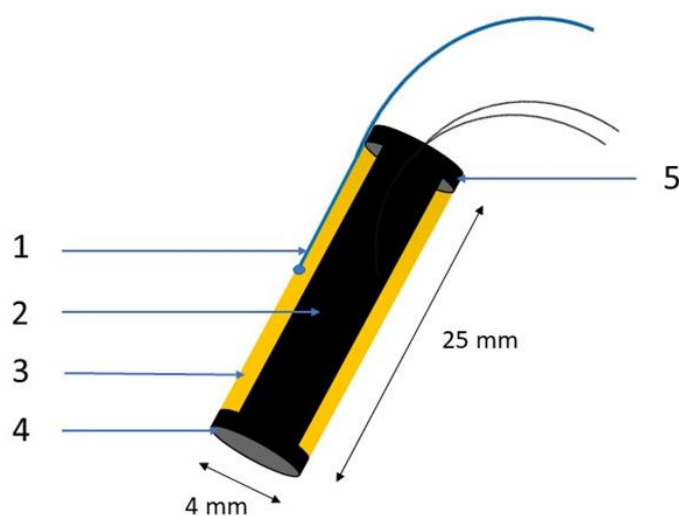


Figure 3. The scheme of the heat transfer probe which is located in the axis of the adsorption bed: 1—thermocouple; 2—cartridge heater; 3—copper case; 4,5—insulation.

The heat probe was constructed of a cartridge heater (2) of known power Q , located in a copper case (3), with the thermocouple (1) placed on its heating surface A . According to the technical data sheet provided by the Sinkoplex Company, the heater power was 0.30 W ($\pm 0.001\text{ W}$), and the heating surface was 0.0003 m^2 ($\pm 0.00001\text{ m}^2$). A second thermocouple was placed at a known distance from the sorption column axis (as shown in Figure 2), and the effective k was calculated from the following relationship:

$$k = \frac{Q}{A \cdot \Delta T}, \left[\frac{\text{W}}{\text{m}^2 \cdot \text{K}} \right] \quad (1)$$

where k is the convective heat transfer coefficient, Q is the power of the heat transfer probe (W), A is the area of the heating surface of the heat transfer probe (m^2), ΔT is the temperature difference between the heat transfer probe's surface and the thermocouple in the volume of sorbent bed (K).

Equation (1) defines the basic method for assessing heat transport effectiveness, focusing on the analysis of the heat transfer coefficient value in laboratory conditions and also in pilot- and large-scale fluidized beds. The maximum measurement error considering the accuracy of the individual components was calculated using the total differential:

$$\Delta k = \left| \frac{\partial k}{\partial Q} \cdot \Delta Q \right| + \left| \frac{\partial k}{\partial A} \cdot \Delta A \right| + \left| \frac{\partial k}{\partial T} \cdot \Delta T \right| \quad (2)$$

The accuracy of the individual measurements shows that the recorded temperature values had the greatest influence on the result of the k calculations. However, due to the maximum value of the measurement error, which ranged from 2.75% to 10.75%, it should be considered that the results of experimental measurements were characterized by good accuracy.

In this study, a conventional packed bed and an innovative fluidized structure were analyzed. During experimental tests, the pressure in the reaction chamber was lower than in the evaporator to force the water vapor to flow when the valve (6, Figure 2) between two sections is opened. It enables the flow of water vapor through the channel (5, Figure 2) connecting the chambers. The minimum fluidization velocity of the solid particles is in the range of 0.43–0.68 m/s [46]. The system operated in transient regimes corresponding to bubbling and circulating fluidized beds (superficial gas velocity: 6.6–14 m/s). Still, in the analyzed set of experimental studies, the bed did not circulate and was held inside the chamber by the grid (2, Figure 2). Under low-pressure conditions, which prevail in the operating cycle of the adsorption chiller, obtaining the fluidized state requires creating a pressure difference between the adsorption chamber and the evaporator to obtain the minimum fluidization velocity by the flowing water vapor. Considering the sample parameters analyzed in these experimental case studies, the optimal initial condition of the fluidization was the achievement of a pressure difference of about 1000 Pa.

2.2. Characteristics of Materials

Preliminary studies [55,57] have confirmed that fluidization improves the heat transfer conditions in the adsorption bed. This paper aims to evaluate average convective heat transfer coefficient values for packed and fluidized bed samples based on the results of experimental studies. The empirical studies involved heat transfer analysis on stationary and fluidized bed models during sorption cycles. Silica gel is a porous adsorption material applied in this study, and it is a material widely available on the market in wholesale quantities. Moreover, it is also an environmentally friendly adsorbent, and according to the literature, it is the best working pair for water as a refrigerant. These parameters make silica gel the most commonly used porous material in adsorption chillers for cooling and desalination [58,59]. The parent silica gel porous material was also supplemented with additives to improve the effective thermal conductivity of the sample. The analyzed beds' samples are described in Table 2. The proposed additives to improve thermal conditions in the deposit indicated in Table 2 were selected based on experimental research and a detailed literature review [23].

Table 2. The composition of adsorption bed samples.

Sample Identification	Composition of Adsorption Bed Sample
S1	Silica gel 100% – reference sample
S2	Silica gel + Aluminum particles 5%
S3	Silica gel + Aluminum particles 15%
S4	Silica gel + Carbon nanotube particles 5%
S5	Silica gel + Carbon nanotube particles 15%

The thermal and physical parameters of the adsorption material, which was a silica gel, are shown in Table 3. The table indicates the sorbent parameters from which adsorption bed samples were prepared and subsequently subjected to the experimental tests described in this paper. Silica gel was chosen as the adsorbent due to the possibility of combining it in the working pair with water as a refrigerant, a highly developed specific surface area of approx. 800 m²/g, and a large total pore volume defined in Table 4.

Table 3. The thermal and physical parameters of the materials.

Material	Particle Size μm	Density kg/m ³	Apparent Density kg/m ³	Bulk Density kg/m ³	Thermal Conductivity W/m·K	Thermal Diffusivity mm ² /s	Sphericity -
Silica gel	160–200	2200	1100	750	0.176	0.137	0.70

Table 4. The sorption parameters of the adsorbent—silica gel.

Specific Surface Area m ² /g	Porosity (ε) -	Av. Pore Diameter nm	Total Pore Volume cm ³ /g (V _p)
800	0.44	2.45	0.404

The crucial sorption parameters of the silica gel are described in Table 4, where the average pore diameter and total pore volume were determined experimentally using the Accelerated Surface Area and Porosimetry System—ASAP 2020 apparatus manufactured by Micromeritics company, Norcross, GA, USA, and the porosity was determined from the following equation:

$$\varepsilon = \frac{V_p}{V_M} \quad (3)$$

where V_p is the total pore volume, cm³/g; V_M is the material volume, cm³/g.

The parameters of additive materials used to improve the thermal properties of the adsorption bed samples are shown in Table 5. Aluminum and carbon nanotubes are characterized by high thermal conductivity, which is a desirable parameter to increase the efficiency of heat and mass transfer.

Table 5. The thermal and physical parameters of the additive materials.

Material	Particle Size μm	Density kg/m ³	Thermal Conductivity W/m·K	Thermal Diffusivity mm ² /s	Sphericity -
Aluminum particles	45–300	2720	237	97.1	0.45
Carbon nanotubes	0.005–10	2600	2320	460	<0.1

3. Results and Discussion

This chapter presents the results and a detailed discussion of the convective heat transfer coefficient calculations for sorption cycles conducted using adsorption bed samples with compositions defined in Table 2. The temperature changes were registered during the experimental tests, which were the basis for calculating the effective heat transfer coefficient according to relation (1).

Experimental tests for the beds' samples defined in Table 2 for fixed and fluidized states were carried out. The water vapor flow due to the pressure difference between the evaporator and the adsorption chamber was used to obtain a fluidized state. Water vapor was generated in the evaporator, and boiling water at 21 °C was achieved by reducing the absolute pressure using the vacuum pump. The sorption processes were carried out in a 2000–2100 Pa pressure range. The initial condition of the adsorption process in the fluidized state was the achievement of a pressure difference between the reaction chamber and the

evaporator of about 1000 Pa, and in the fixed state, about 500 Pa. The adsorption cycles were conducted for about 10 s, as this was the time taken by the pressure equilibration process between the two chambers. After reaching equilibrium, the vapor flow was not occurring. Therefore, the next stage constituted desorption, carried out to desorb water vapor from the sorbent surface and restore the initial pressure difference. The pressures took about 150–250 s to return to their initial state. After this time, the adsorption cycle started again with the opening valve (6, Figure 2) between the two chambers.

For each sorbent sample described in Table 2, seven control cycles were carried out in the fixed and fluidized states. The collected temperature changes were used to calculate the averaged heat transfer coefficient k values. The obtained results are shown in Figures 4–6.

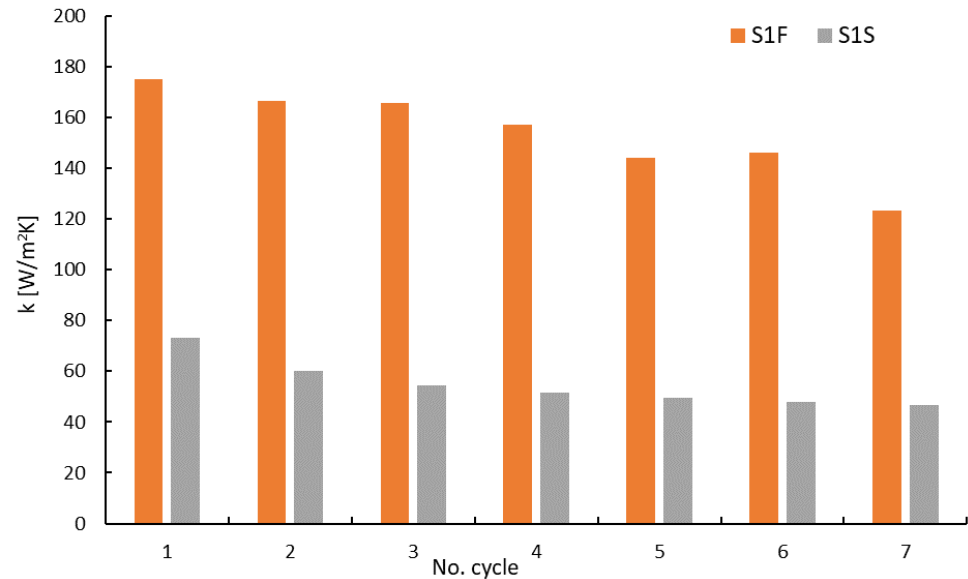


Figure 4. Changes in the average convective heat transfer coefficient values in the following sorption cycles for the reference sample in fluidized (S1F) and fixed (S1S) states. In each cycle, fluidization resulted in an increased convective heat transfer coefficient.

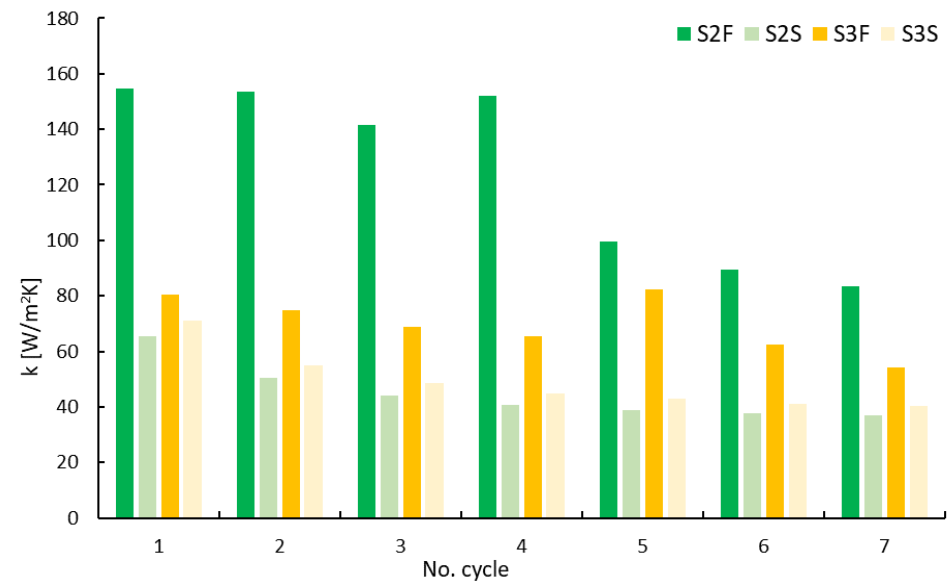


Figure 5. Changes in the average convective heat transfer coefficient values in the following sorption cycles for the bed samples enriched with aluminum particles in fluidized (S2F, S3F) and in fixed (S2S, S3S) states. The highest k values are observed for the sample consisting of silica gel with a 5% addition of aluminum particles.

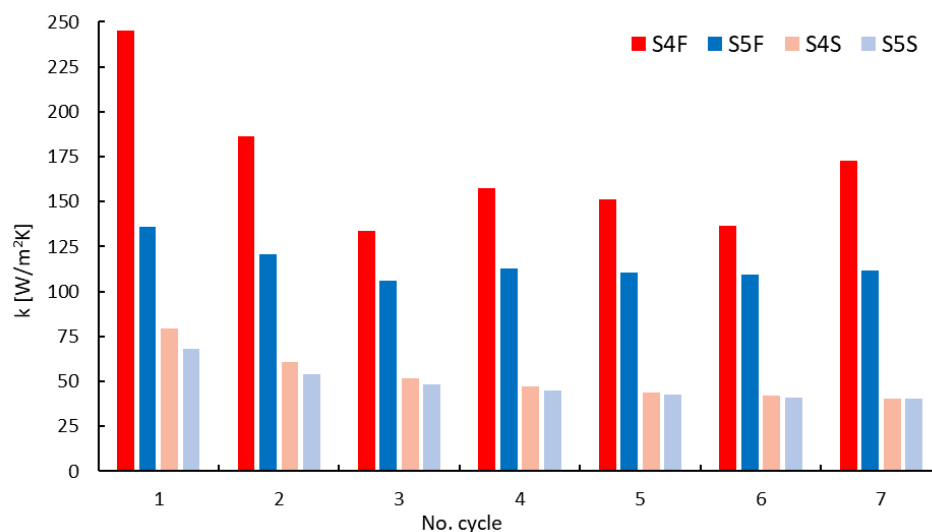


Figure 6. Changes in the average convective heat transfer coefficient values in the following sorption cycles for the bed samples enriched with carbon nanotube particles in fluidized (S4F, S5F) and in fixed (S4S, S5S) states. The highest k values are observed for the sample consisting of silica gel with a 5% addition of carbon nanotubes.

Figure 4 shows the convective heat transfer coefficient k values for the silica gel reference sample. It can be seen that fluidization resulted in an increased convective heat transfer coefficient for each examined adsorption bed sample. For reference adsorption bed samples without thermal additives, the heat transfer coefficient reached a maximum of $70 \text{ W/m}^2 \text{ K}$ in the fixed state, and for the fluidized state, it was approximately $175 \text{ W/m}^2 \text{ K}$. Moreover, in each subsequent adsorption cycle, the fluidized bed was characterized by better thermal conditions than for the fixed state.

The experimental results for adsorption bed samples doped with aluminum particles are depicted in Figure 5. The bed samples contained 5 or 10% aluminum, respectively, and sorption cycles in the fixed and fluidized state were carried out to compare the heat transfer conditions. The highest k values were recorded for sample S2F consisting of silica gel with a 5% addition of aluminum particles.

Figure 6 shows the experimental results for adsorption bed samples doped with carbon nanotubes. As in the case of the aluminum dope tests, the bed samples contained a 5 or 10% additive.

A maximum value of the heat transfer coefficient equal to $245.4 \text{ W/m}^2 \text{ K}$ was achieved in the fluidized state for the S4F sample composed of silica gel with a 5% carbon nanotube additive. However, this high value was registered only in the first adsorption cycle. In subsequent cycles, the value decreased and fluctuated between 130 and $185 \text{ W/m}^2 \text{ K}$. The minimum value of the k equal to $36.9 \text{ W/m}^2 \text{ K}$ was registered in the fixed state for the S2S sample consisting of silica gel with a 5% addition of aluminum particles.

Analysis of experimental results indicates that thermal conditions in the fluidized state are most stable in a homogeneous bed. The results of the adsorption cycles for the doped beds' samples shown in Figures 5 and 6 indicate significant variations in the convective heat transfer coefficient in the following cycles.

Based on the analysis of Tables 3 and 5, which present the physical and thermal properties of the materials forming the adsorption bed samples that were prepared, it can be concluded that the properties of the individual sample components affect the fluctuation in the k coefficient. Minor oscillations of the heat transfer coefficient k during successive adsorption cycles were recorded for the homogeneous sample (S1) made of pure silica gel. In this case, the intensified mixing processes caused by fluidization did not influence the sample structure. In the case of heat-transfer-enhancing additives, the mixing processes affected the stratification of the sample components, resulting in large

fluctuations in the heat transfer coefficient values. Therefore, when designing fluidized silica gel adsorption beds to improve the thermal parameters of the adsorbent, additive materials should be selected based on a similar density and sphericity to the silica gel so that the doped bed forms as homogeneous a layer as possible. Moreover, utilizing carbon nanotubes as thermal additives, it should be noted that nanotubes are characterized by a very high thermal conductivity but only in the longitudinal axis direction. Carbon nanotubes transverse to the axis are insulators.

Analyzing the results presented in Figures 5 and 6, it should also be noted that generally higher values of the heat transfer coefficient were recorded for samples with a 5% admixture of the thermal additives. Therefore, it can be concluded that higher doping does not have a positive effect on heat transfer enhancement in the adsorption bed volume, and the crucial effect in improving the thermal parameters of the bed was caused by the introduction of the fluidized state.

Maintaining high heat transfer coefficient values in the chiller's adsorption bed volume is advantageous due to the lower heating power (HP) consumption during the operating cycle. Reducing the HP consumption without changing the cooling capacity level can influence the increase in the overall efficiency of the adsorption system expressed by the Coefficient of Performance, according to the following relationship:

$$\text{COP} = \frac{\text{CC}}{\text{HP}} = \frac{\dot{m}_c \cdot C_{p_c} \cdot (\Delta T_c)}{\dot{m}_h \cdot C_{p_h} \cdot (\Delta T_h)} \quad (4)$$

where COP is the Coefficient of Performance; CC is the cooling capacity (W); HP is the heating power (W); \dot{m}_c is the mass flow of chilled water (kg/s); C_{p_c} is the specific heat of chilled water (J/kgK); ΔT_c is the temperature difference at the inlet and outlet of the evaporator; \dot{m}_h is the mass flow of hot water (kg/s); C_{p_h} is the specific heat of hot water (J/kgK); and ΔT_h is the temperature difference at the inlet and outlet of the heat exchanger built in the adsorption bed.

COP is the primary parameter used to evaluate the overall performance of an adsorption cooling and desalination system. For the conditions which exist in the adsorption chiller's heat exchanger systems, the specific heat of hot and chilled water corresponds to normal atmospheric conditions, so the changes with pressure are so small that they are ignored to simplify calculations. The ΔT parameters, which are the differences in water temperatures at the inlet and outlet from the heat exchangers built into an evaporator and adsorption bed, respectively, constitute the crucial indicators used to assess the heat transfer conditions. Temperature differences are caused by water evaporation in an evaporator, exothermic adsorption, or endothermic desorption processes conducted in the adsorption beds, depending on the working cycle stage of the adsorption cooling and desalination system. Therefore, the thermal effects accompanying sorption processes require the effective supply or removal of generated heat. An increase in the ΔT value indicates the intensification of heat exchange, which, according to Equation (4), affects the overall efficiency of the system. A higher ΔT for hot water will allow for reducing the hot water flow required to supply the adsorption system. Moreover, the effective desorption of water vapor from the adsorbent surface allows for maintaining a high sorption capacity of the bed in subsequent adsorption cycles.

A higher ΔT for cooling and chilled water will allow for increasing the cooling capacity, which will directly affect the increase in COP of the entire sorption system and will also positively affect the increase in the key parameter characterizing the efficiency of the adsorption bed, i.e., Specific Cooling Power (W/kg) (SCP), expressed by the following equation:

$$\text{SCP} = \frac{\text{CC}}{M_{\text{total}}} \quad (5)$$

where CC is the Cooling Capacity (W) and M_{total} is the total mass of adsorbent (kg).

According to the results for packed bed samples in a fixed state presented in Figures 4–6 (marked with S1S, S2S, S3S, S4S, and S5S symbols), the tendency of the gradual decrease in the heat transfer coefficient is repeated in the following sorption cycles. This relationship applies to all analyzed samples, regardless of their composition. The packed sorbent bed is unevenly saturated as the greatest contact with water vapor is at the bed's lower layers, which, after saturation, no longer generate thermal effects accompanying the sorption processes, which is visible as a decrease in the k parameter value. On the one hand, the lack of mixing processes positively affects the stabilized values of the heat transfer coefficient k of packed samples. On the other hand, the steady state causes uneven adsorption and desorption in the sample volume. Insufficiently desorbed silica gel is characterized by a lower sorption capacity in subsequent cycles, manifested by a decrease in the intensity of mass transfer and heat transfer processes. This is a very unfavorable phenomenon strongly affecting the reduction in the adsorption chiller efficiency used for cooling or desalination.

4. Conclusions

This paper presents an experimental study of heat transfer conditions in packed and fluidized bed sorbent samples. This work also presents innovative guidelines for the design of fluidized adsorption beds. Experimental tests have been carried out utilizing a unique test stand equipped with the Intensified Heat Transfer Adsorption Bed (IHTAB) reactor prototype. The obtained results allowed the analysis of the heat transfer coefficient for various mixtures of adsorption bed samples. The results unambiguously confirmed the improvement in thermal conditions in fluidized beds:

- Fluidization resulted in an increased convective heat transfer coefficient for each examined adsorption bed sample.
- For reference adsorption bed samples without thermal additives (S1S and S1F), the heat transfer coefficient reached a maximum of $70 \text{ W/m}^2 \text{ K}$ in the fixed state, and for the fluidized state, it was approximately $176.5 \text{ W/m}^2 \text{ K}$. Moreover, in each subsequent adsorption cycle, the fluidized bed was characterized by better thermal conditions than the fixed state.
- A minimum value of k equal to $36.9 \text{ W/m}^2 \text{ K}$ was registered in the fixed state for the S2S sample consisting of silica gel with a 5% addition of aluminum particles.
- A maximum value of the heat transfer coefficient equal to $245.4 \text{ W/m}^2 \text{ K}$ was achieved in the fluidized state for the S4F sample composed of silica gel with a 5% carbon nanotube additive.

The tests also revealed an explicit effect of additives improving the thermal bed parameters on the variation in the heat transfer coefficient. This should be considered when designing polydisperse structures of the adsorption beds of adsorption refrigeration and desalination devices. Analyzing the graphs of the heat transfer coefficient in the fluidized state, it can be seen that the results for pure silica gel S1 fluctuated the least. Although additives with a higher thermal conductivity improved the heat transfer in the bed volume, the fluidization process and differences in the density and sphericity of individual sample components caused uneven mixing.

The calculations in this paper were used to analyze the possibility of increasing the COP of the fluidized adsorption chiller compared to the conventional construction of the device. The heat transfer conditions in the adsorption bed volume directly impact many operating parameters of the adsorption device and, in particular, the COP and SCP described in this paper. Therefore, all modifications introduced to adsorption systems aim to increase the convective heat transfer coefficient, because sorption processes are accompanied by thermal effects, which are the system's driving force.

Author Contributions: Conceptualization, J.K. and K.G.; methodology, K.G., A.Z. and A.K.; software, D.S. and M.S.; validation, J.K., K.G., R.Š. and T.C.; formal analysis, M.S., R.Š. and T.C.; investigation, A.K., A.Z. and D.S.; resources, J.K. and W.N.; data curation, K.G., A.Z. and A.K.; writing—original draft preparation, K.G.; writing—review and editing, J.K. and M.S.; visualization, K.G.; supervision, J.K., M.S. and W.N.; project administration, J.K.; funding acquisition, J.K. and K.G. All authors have read and agreed to the published version of the manuscript.

Funding: This research was funded by the National Science Centre, Poland, project No. 2018/29/B/ST8/00442. The support is gratefully acknowledged.

Data Availability Statement: Data are contained within the article.

Conflicts of Interest: The authors declare no conflicts of interest.

Glossary

AB	Absorption
AD	Adsorption
CC	Cooling Capacity, W
C_{p_c}	specific heat of chilled water, J/kgK
C_{p_h}	specific heat of hot water, J/kgK
CFB	Circulating Fluidized Bed
COP	Coefficient of Performance
F	Fluidized state
HP	Heating Power, W
IHTAB	Intensified Heat Transfer Adsorption Bed
k	convective heat transfer coefficient, W/m ² ·K
M_{total}	total mass of adsorbent kg,
\dot{m}_c	a mass flow of chilled water, kg/s
\dot{m}_h	a mass flow of hot water, kg/s
S	Stationary state (fixed)
SCP	Specific Cooling Power, W/kg
S1–S5	Samples' identification
ΔT_c	temperature difference at the inlet and outlet of the evaporator;
ΔT_h	temperature difference at the inlet and outlet of the heat exchanger built in the adsorption bed;
ρ_{bulk}	Bulk density of the silica gel, kg/m ³
ρ_{app}	Apparent density of the silica gel, kg/m ³
ϵ	porosity of the silica gel, -

References

1. Windram, C. Climate change policy & global energy projections—After Kyoto. *Renew. Energy Technol. Policies Sustain. Dev.* **1999**, 341–344.
2. Chepeliev, M.; van der Mensbrugghe, D. Global fossil-fuel subsidy reform and Paris Agreement. *Energy Econ.* **2020**, *85*, 104598. [[CrossRef](#)]
3. Mundaca, G. How much can CO₂ emissions be reduced if fossil fuel subsidies are removed? *Energy Econ.* **2017**, *64*, 91–104. [[CrossRef](#)]
4. He, B.; Pan, Q.J.; Deng, Z.Q. Product carbon footprint for product life cycle under uncertainty. *J. Clean. Prod.* **2018**, *187*, 459–472. [[CrossRef](#)]
5. Chen, J.D.; Fan, W.; Li, D.; Liu, X.; Song, M.L. Driving factors of global carbon footprint pressure: Based on vegetation carbon sequestration. *Appl. Energy* **2020**, *267*, 114914. [[CrossRef](#)]
6. Wu, J.Z.; Liu, G.H.; Marson, A.; Fedele, A.; Scipioni, A.; Manzardo, A. Mitigating environmental burden of the refrigerated transportation sector: Carbon footprint comparisons of commonly used refrigeration systems and alternative cold storage systems. *J. Clean. Prod.* **2022**, *372*, 133514. [[CrossRef](#)]
7. Di Filippo, R.; Bursi, O.S.; Di Maggio, R. Global warming and ozone depletion potentials caused by emissions from HFC and CFC banks due structural damage. *Energy Build.* **2022**, *273*, 112385. [[CrossRef](#)]
8. Ali, E.S.; Askalany, A.A.; Harby, K.; Diab, M.R.; Alsaman, A.S. Adsorption desalination-cooling system employing copper sulfate driven by low grade heat sources. *Appl. Therm. Eng.* **2018**, *136*, 169–176. [[CrossRef](#)]
9. Mitra, S.; Thu, K.; Saha, B.B.; Dutta, P. Performance evaluation and determination of minimum desorption temperature of a two-stage air cooled silica gel/water adsorption system. *Appl. Energy* **2017**, *206*, 507–518. [[CrossRef](#)]

10. Pereira, M.A.; Marques, R.C. Sustainable water and sanitation for all: Are we there yet? *Water Res.* **2021**, *207*, 117765. [[CrossRef](#)]
11. Hua, W.S.; Xu, H.J.; Xie, W.H. Review on adsorption materials and system configurations of the adsorption desalination applications. *Appl. Therm. Eng.* **2022**, *204*, 117958. [[CrossRef](#)]
12. Zohir, A.E.; Ali, E.S.; Farid, A.M.; Elshaer, R.N.; Mohammed, R.H.; Alsaman, A.S.; El-Ghetany, H.H.; Askalany, A.A. A state-of-the-art of experimentally studied adsorption water desalination systems. *Int. J. Energy Environ. Eng.* **2023**, *14*, 573–599. [[CrossRef](#)]
13. Ghazy, M.; Ibrahim, E.M.M.; Mohamed, A.S.A.; Askalany, A.A. Experimental investigation of hybrid photovoltaic solar thermal collector (PV/T)-adsorption desalination system in hot weather conditions. *Energy* **2022**, *254*, 124370. [[CrossRef](#)]
14. Ben Hamida, M.B.; Alshammari, F.; Alatawi, I.; Alhadri, M.; Almeshaal, M.A.; Hajlaoui, K. Potential Of Tubular Solar Still With Rectangular Trough For Water Production Under Vacuum Condition. *Therm. Sci.* **2022**, *26*, 4271–4283.
15. Ben Hamida, M.B. Numerical analysis of tubular solar still with rectangular and cylindrical troughs for water production under vacuum. *J. Taibah Univ. Sci.* **2023**, *17*, 2159172. [[CrossRef](#)]
16. Wang, R.Z.; Oliveira, R.G. Adsorption refrigeration—An efficient way to make good use of waste heat and solar energy. *Prog. Energy Combust. Sci.* **2006**, *32*, 424–458. [[CrossRef](#)]
17. Tokarev, M.M.; Gordeeva, L.G.; Grekova, A.D.; Aristov, Y.I. Adsorption cycle “heat from cold” for upgrading the ambient heat: The testing a lab-scale prototype with the composite sorbent CaClBr/silica. *Appl. Energy* **2018**, *211*, 136–145. [[CrossRef](#)]
18. Lim, K.; Lee, S.; Lee, C. An experimental study on the thermal performance of ground heat exchanger. *Exp. Therm. Fluid Sci.* **2007**, *31*, 985–990. [[CrossRef](#)]
19. Chen, W.D.; Chua, K.J. Parameter analysis and energy optimization of a four-bed, two-evaporator adsorption system. *Appl. Energy* **2020**, *265*, 114842. [[CrossRef](#)]
20. Sah, R.P.; Choudhury, B.; Das, R.K. Study of a two-bed silica gel-water adsorption chiller: Performance analysis. *Int. J. Sustain. Energy* **2018**, *37*, 30–46. [[CrossRef](#)]
21. Alsarayreh, A.A.; Al-Maaitah, A.; Attarakih, M.; Bart, H.J. Performance Analysis of Variable Mode Adsorption Chiller at Different Recooling Water Temperatures. *Energies* **2021**, *14*, 3871. [[CrossRef](#)]
22. Sidhareddy, M.; Tiwari, S.; Phelan, P.; Bellos, E. Comprehensive review on adsorption cooling systems and its regeneration methods using solar, ultrasound, and microwave energy. *Int. J. Refrig.* **2023**, *146*, 174–201. [[CrossRef](#)]
23. Pajdak, A.; Kulakowska, A.; Liu, J.F.; Berent, K.; Kudasik, M.; Krzywanski, J.; Kalawa, W.; Sztékler, K.; Skoczylas, N. Accumulation and Emission of Water Vapor by Silica Gel Enriched with Carbon Nanotubes CNT-Potential Applications in Adsorption Cooling and Desalination Technology. *Appl. Sci.* **2022**, *12*, 5644. [[CrossRef](#)]
24. Boruta, P.; Bujok, T.; Sztékler, K. Adsorbents, Working Pairs and Coated Beds for Natural Refrigerants in Adsorption Chillers-State of the Art. *Energies* **2021**, *14*, 4707. [[CrossRef](#)]
25. Shaaban, M.; Elsheniti, M.B.; Rezk, A.; Elhelw, M.A.; Elsamni, O.A. Performance investigation of adsorption cooling and desalination systems employing thermally enhanced copper foamed bed coated with SAPO-34 and CPO-27(Ni). *Appl. Therm. Eng.* **2022**, *205*, 118056. [[CrossRef](#)]
26. Grabowska, K.; Sztékler, K.; Krzywanski, J.; Sosnowski, M.; Stefanski, S.; Nowak, W. Construction of an innovative adsorbent bed configuration in the adsorption chiller part 2. experimental research of coated bed samples. *Energy* **2021**, *215*, 119123. [[CrossRef](#)]
27. Sharafian, A.; Fayazmanesh, K.; McCague, C.; Bahrami, M. Thermal conductivity and contact resistance of mesoporous silica gel adsorbents bound with polyvinylpyrrolidone in contact with a metallic substrate for adsorption cooling system applications. *Int. J. Heat Mass Transf.* **2014**, *79*, 64–71. [[CrossRef](#)]
28. Li, K.Y.; Luo, W.J.; Tsai, B.Y.; Kuan, Y.D. Performance Analysis of Two-Stage Solid Desiccant Densely Coated Heat Exchangers. *Sustainability* **2020**, *12*, 7357. [[CrossRef](#)]
29. Panigrahi, B.; Chen, Y.S.; Luo, W.J.; Wang, H.W. Dehumidification Effect of Polymeric Superabsorbent SAP-LiCl Composite Desiccant-Coated Heat Exchanger with Different Cyclic Switching Time. *Sustainability* **2020**, *12*, 9673. [[CrossRef](#)]
30. Sosnowski, M. Evaluation of Heat Transfer Performance of a Multi-Disc Sorption Bed Dedicated for Adsorption Cooling Technology. *Energies* **2019**, *12*, 4660. [[CrossRef](#)]
31. Papakokinos, G.; Castro, J.; Oliet, C.; Oliva, A. Computational investigation of the hexagonal honeycomb adsorption reactor for cooling applications. *Appl. Therm. Eng.* **2022**, *202*, 117807. [[CrossRef](#)]
32. Ilis, G.G.; Demir, H.; Moberi, M.; Saha, B.B. A new adsorbent bed design: Optimization of geometric parameters and metal additive for the performance improvement. *Appl. Therm. Eng.* **2019**, *162*, 114270. [[CrossRef](#)]
33. Papakokinos, G.; Castro, J.; López, J.; Oliva, A. A generalized computational model for the simulation of adsorption packed bed reactors—Parametric study of five reactor geometries for cooling applications. *Appl. Energy* **2019**, *235*, 409–427. [[CrossRef](#)]
34. Jodlowski, P.J.; Kurowski, G.; Skoczylas, N.; Pajdak, A.; Kudasik, M.; Jedrzejczyk, R.J.; Kuterasinski, L.; Jelen, P.; Sitarz, M.; Li, A.; et al. Silver and copper modified zeolite imidazole frameworks as sustainable methane storage systems. *J. Clean. Prod.* **2022**, *352*, 131638. [[CrossRef](#)]
35. Freni, A.; Sapienza, A.; Glaznev, I.S.; Aristov, Y.I.; Restuccia, G. Experimental testing of a lab-scale adsorption chiller using a novel selective water sorbent “silica modified by calcium nitrate”. *Int. J. Refrig. Rev. Int. Du Froid* **2012**, *35*, 518–524. [[CrossRef](#)]
36. Panigrahi, B.; Wang, H.W.; Luo, W.J.; Chou, Y.C.; Chen, J.J. Comparative analysis of the static and dynamic dehumidification performance of metal-organic framework materials. *Sci. Technol. Built Environ.* **2023**, *29*, 323–338. [[CrossRef](#)]

37. Bahrehmand, H.; Khajepour, M.; Bahrami, M. Finding optimal conductive additive content to enhance the performance of coated sorption beds: An experimental study. *Appl. Therm. Eng.* **2018**, *143*, 308–315. [[CrossRef](#)]
38. Li, M.L.; Zhao, Y.N.; Long, R.; Liu, Z.C.; Liu, W. Gradient porosity distribution of adsorbent bed for efficient adsorption cooling. *Int. J. Refrig.* **2021**, *128*, 153–162. [[CrossRef](#)]
39. Khan, M.Z.I.; Alam, K.C.A.; Saha, B.B.; Akisawa, A.; Kashiwagi, T. Performance evaluation of multi-stage, multi-bed adsorption chiller employing re-heat scheme. *Renew. Energy* **2008**, *33*, 88–98. [[CrossRef](#)]
40. Zajackowski, B. Optimizing performance of a three-bed adsorption chiller using new cycle time allocation and mass recovery. *Appl. Therm. Eng.* **2016**, *100*, 744–752. [[CrossRef](#)]
41. Nikbakhti, R.; Wang, X.L.; Chan, A. Performance optimization of an integrated adsorption-absorption cooling system driven by low-grade thermal energy. *Appl. Therm. Eng.* **2021**, *193*, 117035. [[CrossRef](#)]
42. Nikbakhti, R.; Iranmanesh, A. Potential application of a novel integrated adsorption-absorption refrigeration system powered with solar energy in Australia. *Appl. Therm. Eng.* **2021**, *194*, 117114. [[CrossRef](#)]
43. Albaik, I.; Al-Dadah, R.; Mahmoud, S.; Solmaz, I. Non-equilibrium numerical modelling of finned tube heat exchanger for adsorption desalination/cooling system using segregated solution approach. *Appl. Therm. Eng.* **2021**, *183*, 116171. [[CrossRef](#)]
44. Komeilibirjandi, A.; Raffiee, A.H.; Maleki, A.; Nazari, M.A.; Shadloo, M.S. Thermal conductivity prediction of nanofluids containing CuO nanoparticles by using correlation and artificial neural network. *J. Therm. Anal. Calorim.* **2020**, *139*, 2679–2689. [[CrossRef](#)]
45. Grabowska, K.; Sosnowski, M.; Krzywanski, J.; Sztekler, K.; Kalawa, W.; Zylka, A.; Nowak, W. The Numerical Comparison of Heat Transfer in a Coated and Fixed Bed of an Adsorption Chiller. *J. Therm. Sci.* **2018**, *27*, 421–426. [[CrossRef](#)]
46. Krzywanski, J.; Skrobek, D.; Zylka, A.; Grabowska, K.; Kulakowska, A.; Sosnowski, M.; Nowak, W.; Blanco-Marigorta, A.M. Heat and mass transfer prediction in fluidized beds of cooling and desalination systems by AI approach. *Appl. Therm. Eng.* **2023**, *225*, 120200. [[CrossRef](#)]
47. Krzywanski, J.; Czakiert, T.; Nowak, W.; Shimizu, T.; Zylka, A.; Idziak, K.; Sosnowski, M.; Grabowska, K. Gaseous emissions from advanced CLC and oxyfuel fluidized bed combustion of coal and biomass in a complex geometry facility: A comprehensive model. *Energy* **2022**, *251*, 123896. [[CrossRef](#)]
48. Chiang, Y.C.; Chen, C.H.; Chen, S.L. Circulating inclined fluidized beds with application for desiccant dehumidification systems. *Appl. Energy* **2016**, *175*, 199–211. [[CrossRef](#)]
49. Krzywanski, J.; Sztekler, K.; Szubel, M.; Siwek, T.; Nowak, W.; Mika, L. A Comprehensive, Three-Dimensional Analysis of a Large-Scale, Multi-Fuel, CFB Boiler Burning Coal and Syngas. Part 2. Numerical Simulations of Coal and Syngas Co-Combustion. *Entropy* **2020**, *22*, 856. [[CrossRef](#)] [[PubMed](#)]
50. Khaled, G.; Bourouina-Bacha, S.; Sabiri, N.E.; Tighzert, H.; Kechroud, N.; Bourouina, M. Simplified correlations of axial dispersion coefficient and porosity in a solid-liquid fluidized bed adsorber. *Exp. Therm. Fluid Sci.* **2017**, *88*, 317–325. [[CrossRef](#)]
51. Qian, S.X.; Ling, J.Z.; Muehlbauer, J.; Hwang, Y.H.; Radermacher, R. Study on high efficient heat recovery cycle for solid-state cooling. *Int. J. Refrig. Rev. Int. Du Froid* **2015**, *55*, 102–119. [[CrossRef](#)]
52. Qi, B.J.; Yan, Y.; Zhang, W.B.A.; Wang, X.Y. Measurement of biomass moisture content distribution in a fluidised bed dryer through electrostatic sensing and digital imaging. *Powder Technol.* **2021**, *388*, 380–392. [[CrossRef](#)]
53. Lasek, L.; Zylka, A.; Krzywanski, J.; Skrobek, D.; Sztekler, K.; Nowak, W. Review of Fluidized Bed Technology Application for Adsorption Cooling and Desalination Systems. *Energies* **2023**, *16*, 7311. [[CrossRef](#)]
54. Krzywanski, J.; Grabowska, K.; Sosnowski, M.; Zylka, A.; Kulakowska, A.; Czakiert, T.; Sztekler, K.; Wesolowska, M.; Nowak, W. Heat Transfer in Adsorption Chillers with Fluidized Beds of Silica Gel, Zeolite, and Carbon Nanotubes. *Heat Transf. Eng.* **2021**, *43*, 172–182. [[CrossRef](#)]
55. Grabowska, K.; Zylka, A.; Kulakowska, A.; Skrobek, D.; Krzywanski, J.; Sosnowski, M.; Ciesielska, K.; Nowak, W. Experimental Investigation of an Intensified Heat Transfer Adsorption Bed (IHTAB) Reactor Prototype. *Materials* **2021**, *14*, 3520. [[CrossRef](#)]
56. Rozenek, M. *Manual of the Experimental Test Stand; Automatic Solutions sp. z o.o.*: Marcinowice, Poland, 2019.
57. Dawoud, B. Water vapor adsorption kinetics on small and full scale zeolite coated adsorbents; A comparison. *Appl. Therm. Eng.* **2013**, *50*, 1645–1651. [[CrossRef](#)]
58. Younes, M.M.; El-Sharkawy, I.I.; Kabeel, A.E.; Saha, B.B. A review on adsorbent-adsorbate pairs for cooling applications. *Appl. Therm. Eng.* **2017**, *114*, 394–414. [[CrossRef](#)]
59. Shmroukh, A.N.; Ali, A.H.H.; Ookawara, S. Adsorption working pairs for adsorption cooling chillers: A review based on adsorption capacity and environmental impact. *Renew. Sustain. Energy Rev.* **2015**, *50*, 445–456. [[CrossRef](#)]

Disclaimer/Publisher's Note: The statements, opinions and data contained in all publications are solely those of the individual author(s) and contributor(s) and not of MDPI and/or the editor(s). MDPI and/or the editor(s) disclaim responsibility for any injury to people or property resulting from any ideas, methods, instructions or products referred to in the content.